Prolific nitrite re-oxidation across the Eastern Tropical North Pacific Ocean

Natalya Evans[1], Juliana Tichota[1], James W. Moffett[1], and Allan H. Devol[2,*]

[1]Department of Biological Sciences, University of Southern California, Los Angeles, California

[2]School of Oceanography, University of Washington, Seattle, Washington

*Corresponding author at: School of Oceanography, University of Washington, Seattle, Washington, devol@uw.edu

Abstract

Marine Oxygen Deficient Zones serve as hotspots for the loss of fixed nitrogen for the world's oceans, and fixed nitrogen limits primary productivity in large expanses of the ocean. This fixed nitrogen loss occurs primarily through denitrification, where the stepwise reduction of nitrate to nitrite and ultimately to dinitrogen gas is coupled to organic matter oxidation. Nitrite, the first intermediate in denitrification, can also be re-oxidized back to nitrate in a reaction by chemoautotrophic microbes. Nitrite's partitioning between reduction and oxidation determines if marine fixed nitrogen is lost or recycled. Nitrite oxidation in anoxic waters has been previously studied through stable and tracer isotope experiments, but the difficulty of these measurements has limited their geographical distribution and therefore requires extrapolation to understand their impact on the nitrogen cycling. Using basin-scale data, we analyze the progression of nutrients within the three water masses that feed the Eastern Tropical North Pacific Oxygen Deficient Zone. Significant deviations from the expected stoichiometry for denitrification demonstrate that 79% of the nitrite produced in the upper region of the Oxygen Deficient Zone is re-oxidized, whereas only 54% of the nitrite produced in the lower region of the Oxygen Deficient Zone is re-oxidized. These large estimates for nitrite re-oxidation reveal significant fixed nitrogen recycling across the Eastern Tropical North Pacific.

Introduction

Denitrification consists of a series of reduction reactions that convert fixed nitrogen, which is generally available for biological reactions, to dinitrogen gas, which is unavailable for these reactions. These reactions occur within the oxygen deficient layers of the water column within marine Oxygen Deficient Zones (ODZs) as well as within marine sediments. Denitrification is the

primary process removing fixed nitrogen in the marine fixed nitrogen budget (Brandes and Devol 2002) and therefore an important regulatory control on marine productivity. During denitrification, organic matter is oxidized to carbon dioxide and inorganic phosphate is produced from organic phosphorus compounds, causing a stoichiometric decrease in nitrate and increases in total carbon as well as phosphate. While the inorganic C:N:P stoichiometry for aerobic respiration of organic matter is 106:16:1 and commonly referred to as Redfield stoichiometry, similar Redfield relationships exist for other metabolic pathways. The inorganic C:N:P stoichiometry during denitrification from nitrate to dinitrogen gas is 106:-94.4:1 (Froelich et al. 1979), and estimates of fixed nitrogen loss commonly rely on comparing nitrate and phosphate concentrations, such as N* (Gruber and Sarmiento 1997).

The first reaction in the denitrification process is dissimilatory reduction of nitrate to nitrite. As denitrification continues, further reduction of this nitrogen converts nitrite to a series of intermediates consisting of nitric oxide and nitrous oxide before finally converting it to dinitrogen gas. Due to their more widespread biological availability, nitrate and nitrite are often considered "fixed nitrogen", unlike nitric/nitrous oxide and dinitrogen gas (Chang et al. 2014). In the canonical denitrification process, nitrate proceeds sequentially through these reduction reactions, however, studies have found that nitrite is frequently re-oxidized to nitrate within ODZs. The pathways for nitrite oxidation are currently not well-defined and spatially heterogenous throughout ODZs (Sun et al. 2021), with potential oxidizing agents such as oxygen, iodate, Mn^{4+} and even nitrite itself through a dismutation reaction (Babbin et al. 2017, 2020). An ammonia-oxidizing archaeon was recently discovered that is able to produce oxygen in dark, anoxic ocean waters (Kraft et al. 2022), which could provide an oxygen source within the anoxic ODZ. Previous studies into the fate of nitrite in the Pacific ODZs found that the vertical structure of the ODZ influenced the relative amount of oxidation as well as the oxidizing agents of nitrite re-oxidation. Elevated nitrite re-oxidation has been found in the edges of ODZs, surrounding the oxygen deficient layer that primarily denitrifies (Casciotti et al. 2013), due to the flux of trace amounts of oxygen into the ETNP ODZ. Nevertheless, nitrite oxidation can occur anaerobically (Sun et al. 2021), as the additional oxygen atom in nitrate versus nitrite is derived from water (DiSpirito and Hooper 1986).

Recent isotopic tracer and stable isotope studies have measured the rates of nitrite oxidation and, in some studies, estimated the relative partitioning of nitrite to reduction versus re-oxidation. In the Costa Rica Dome, the southern side of the Eastern Tropical North Pacific (ETNP) ODZ,

50% of the nitrite was re-oxidized (Buchwald et al. 2015). Data from near the center of the ETNP ODZ also found consistently high rates of nitrite oxidation throughout the ODZ, including the oxygen deficient layer (Babbin et al. 2020) as well as the upper oxycline (Peng et al. 2015). Due to the laborious nature of these measurements (Garcia-Robledo et al. 2016), they are still scarce, such that estimates of the impact of nitrite oxidation across the ETNP ODZ requires significant extrapolation. Fortunately, nitrite oxidation does not stoichiometrically influence inorganic phosphate (Anderson et al. 1982) because nitrite oxidizers are chemoautotrophs (Lipschultz et al. 1990). We analyze deviations from 106:-94.4:1 C:N:P stoichiometry (Froelich et al. 1979) to estimate the magnitude of chemical transformations occurring within the water masses of the Eastern Tropical North Pacific. We focus on positive deviation in the -94.4 N value in the 106:-94.4:1 C:N:P stoichiometry (Froelich et al. 1979), which has three potential explanations. First, nitrite is being re-oxidized back to nitrate, which impacts both the C:N and N:P stoichiometries. Second, the proportion of carbon relative to nitrogen in organic matter being oxidized is lower (Van Mooy et al. 2002), decreasing the C:N and C:P stoichiometries. Third, carbon fixation through both photo- and chemo-autotrophy as well as carbonate dissolution occurs, which lowers or elevates the C:N and C:P stoichiometries. Only nitrite re-oxidation impacts the N:P stoichiometry without significantly changing the C:P stoichiometry, because carbon fixation will be accompanied by phosphate uptake for autotrophs. This behavior suggests that the C:P stoichiometry identifies the magnitude of the second and third processes on these water masses. Therefore, positive deviations in the N:P stoichiometries relative to the C:P stoichiometries indicate ratio of nitrite that is re-oxidized rather than further reduced. This ratio can then be applied to determine the degree that calculations of fixed nitrogen loss based on inorganic nitrogen versus phosphate overestimate denitrification. Here, we analyzed the progression of nutrients within the three water masses that feed the Eastern Tropical North Pacific Oxygen Deficient Zone to determine the relative importance of nitrite oxidation compared to nitrite reduction.

Methods

We analyzed Pacific-wide data products spanning wide spatial and temporal ranges. Gridded data from World Ocean Atlas 2013 (Garcia et al. 2013) were acquired via the WOA13_1.00deg_1955-2012_Annual file available from the Ocean Data View web portal (https://odv.awi.de/data/ocean/world-ocean-atlas-2013/). Available temperature, salinity, oxygen,

phosphate, and nitrate, and dissolved inorganic carbon were extracted from the World Ocean Database 2018 (Garcia et al. 2013) using the WODselect tool (https://www.ncei.noaa.gov/access/world-ocean-database-select/dbsearch.html). Both the WOA13 and the WOD18 data were processed and visualized with Ocean Data View version 5.1.7 (Schlitzer 2020) and MATLAB R2018b (The MathWorks, Inc. 2018). TEOS-10 (http://www.teos-10.org/software.htm) (T. J. McDougall and Barker 2011) was used to convert in situ temperature and salinity to conservative temperature and absolute salinity, as well as calculate potential density anomaly, using IBM ILOG CPLEX Optimization Studio V12.8.0 as an optimizer. Nutrient ratios for each water mass were calculated using Type II linear regressions with pre-existing code (Glover et al. 2011). All data were plotted, but outliers were excluded from these linear regressions. With regards to visualizing data, the viridis colormap was selected for scientific use of color and accessibility (Crameri et al. 2020), rather than the "odv" option which is used as default.

We subdivided this data into the three water masses that compose the ETNP ODZ using conservative parameters centered around water mass definitions specified in a water mass analysis of this region (Evans et al. 2020). Table 1 provides these specifications, which are generously wide in an effort to include sufficient data that outliers do not interfere with calculations. With these water mass subsets, we analyzed the C:N:P regeneration ratios resulting from non-aerobic processes. The percentages of nitrite re-oxidized were calculated using Eq. (1) or Eq. (2) for WOD18 or WOA13 data, respectively.

	13CW		NEPIW		AAIW	
	Min	Max	Min	Max	Min	Max
θ/ºC	12.5	13.5	9	10	5	6
S_A/g kg^{-1}	34.8	35.2	34.7	34.85	34.67	34.72
σ_θ/kg m^{-3}	26.2	26.4	26.7	26.9	27.2	27.3
*Latitude/ºN	0	n/a	0	n/a	0	n/a
*NO_3^-/µmol kg^{-1}	15	n/a	n/a	n/a	n/a	n/a

Table 1) Ranges for filtering WOA13 and WOD18 data into coherent water masses. Starred variables were only used to filter the data for linear regression of nutrient ratios in Fig. 2, not for geographic distributions in Fig. 1.

$$NO_2^- \ oxidized\ (\%) = 100\left(\frac{(Total\ CO_2{:}NO_3^-)_i - (-1.12)}{(Total\ CO_2{:}NO_3^-)_i}\right) \quad (1)$$

$$NO_2^- \ oxidized\ (\%) = 100\left(\frac{-94.4 - (NO_3^-{:}PO_4^{3-})_i}{-94.4}\right) \quad (2)$$

Source waters to the Pacific Oxygen Deficient Zones

Three water masses compose both the Pacific ODZs, with slight differences between the ETNP and Eastern Tropical South Pacific (ETSP) (Evans et al. 2020). In the ETNP, these water masses are the 13 ºC Water (13CW), Northern Equatorial Pacific Intermediate Water (NEPIW), and Antarctic Intermediate Water (AAIW). Fig. 1 depicts the geographical extent of each water mass using subsets of World Ocean Atlas 2013 gridded data (WOA13) based on the temperature and salinity of each water mass, listed in Table 1. The 13CW subset was selected to be slightly deeper than that found in Evans et al. (2020). This decision is based off the results of particle backtracking into the ETNP ODZ, which found the entry of this water mass through the southern boundary of the ODZ slightly deeper (Margolskee et al. 2019). In addition, while other references (Bostock et al. 2010) define the center of the NEPIW and its southern counterpart, SEPIW, closer to σ_θ=27 kg m^{-3}, the Northern Equatorial Undercurrent Jets that inject the NEPIW into the ETNP ODZ are centered at σ_θ=26.8 kg m^{-3} (Qiu et al. 2013; Margolskee et al. 2019). To represent the waters that feed the ETNP ODZ, we adjusted our subset to be shallower, even though this process selects specifically the upper region of these water masses.

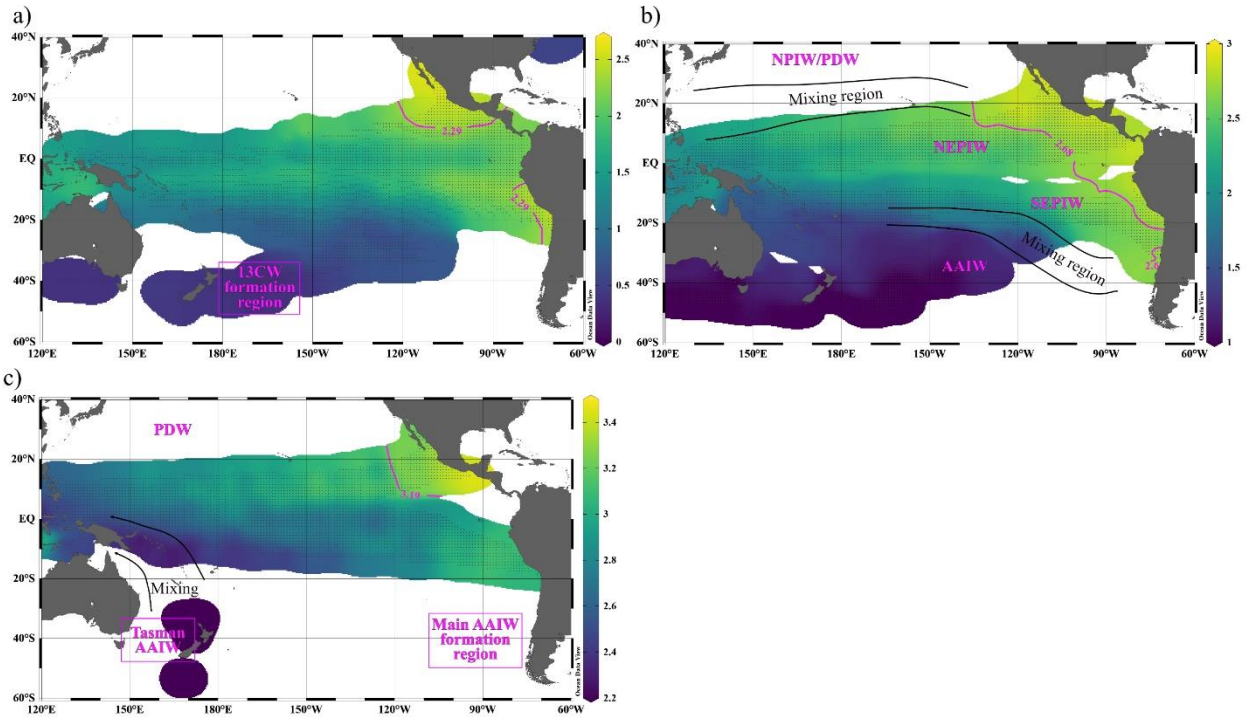

Fig. 1) Maps of (a) 13CW, (b) NEPIW/SEPIW, and (c) AAIW, depicting PO_4^{3-}/µmol kg^{-1}. The contour line depicts the concentration past which anaerobic respiration appears to begin, as given in Fig. 2. Water mass formation sources are noted.

In Fig. 1, the phosphate concentrations of each water mass are used to depict how the water masses age as they are transported from their source regions to the Pacific ODZs. The purple contour represents the approximate location where the signal of anaerobic metabolisms can be detected. This concentration is identified in Fig. 2 and described in surrounding text, however these phosphate concentrations are based on the ETNP ODZ and do not reflect the ETSP as well. Nevertheless, these plots confirm that the Pacific ODZs share coherent source water masses, as well as visualize the flow paths for these water masses entering the ETNP ODZ. While these source water masses are coherent between Pacific ODZs, there are slight differences in the water masses between each ODZ. For example, the Equatorial Pacific Intermediate Water that consists of NEPIW and SEPIW is formed by the subsurface mixing of primarily Pacific Deep Water (PDW) and AAIW with some NPIW. Since the AAIW has far higher dissolved oxygen concentrations than the PDW, the SEPIW remains oxygenated and therefore the ETSP ODZ is shallower than the ETNP ODZ (Kwiecinski and Babbin 2021).

The 13CW enters from the south via the Northern Subsurface Countercurrent (Fiedler and Talley 2006; Margolskee et al. 2019), and references for these paths and source regions are

described further in Evans et al. (2020), except the AAIW. The AAIW has several formation regions across the Southern Hemisphere, two of which are displayed in Fig. 1c; however, the geographical extent of this water mass definition does not intersect directly with either of these locations. Instead, the AAIW observed in both the ETNP and ETSP ODZ is likely a form of AAIW that has been mixed with other water masses, likely PDW, as Tasman Sea AAIW has a northwestern mixing location (Qu and Lindstrom 2004; Bostock et al. 2013).

Basin-scale quantification of nitrite re-oxidation

While the ocean's fixed nitrogen budget depends on the relative partitioning of nitrite lost via further denitrification versus recycled via oxidation, measurements of nitrite reactions are particularly challenging. Investigations into nitrite oxidation typically extrapolate results based on a small number of cruises with limited spatiotemporal sampling. To overcome these limitations, we analyzed WOA13 data for nitrate:phosphate ratios within the source water masses for the ETNP ODZ. If each step of denitrification occurs irreversibly, the nitrate:phosphate ratio should be -94.4:1 for each water mass. However, the 13CW, NEPIW, and AAIW had slopes of -20±1, -43±1, and -34±3, appropriately. These data are presented in Fig. 2a and Table 2. Since WOA13 did not contain carbon data, we verified that these deviations in the nitrate:phosphate ratio were due to nitrate by comparing regressions of both nutrients against total inorganic carbon data from WOD18, presented in Fig. 2c and 2d, appropriately. We found that carbon:phosphate deviated less than 12% from the expected 106:1 ratio and this deviation was positive for the NEPIW and AAIW but not the 13CW. These positive deviations are likely due to carbonate dissolution, since this is one of the few processes that increases the carbon:phosphate ratio and it can occur within these deeper waters (Hernandez-Ayon et al. 2019). In contrast, the negative deviation in the 13CW occurs due to carbon fixation near the base of the euphotic zone, which the 13CW can mix into. Despite the fact that carbon:phosphate ratios deviated by less than 12%, the carbon:nitrate ratios were -3±0.4 and -3±0.2 for 13CW and NEPIW, appropriately. These ratios of approximately -3 are significantly lower than the -1.12 predicted from reaction stoichiometry (Froelich et al. 1979), indicating that denitrifying a single nitrate requires almost three times the carbon expected.

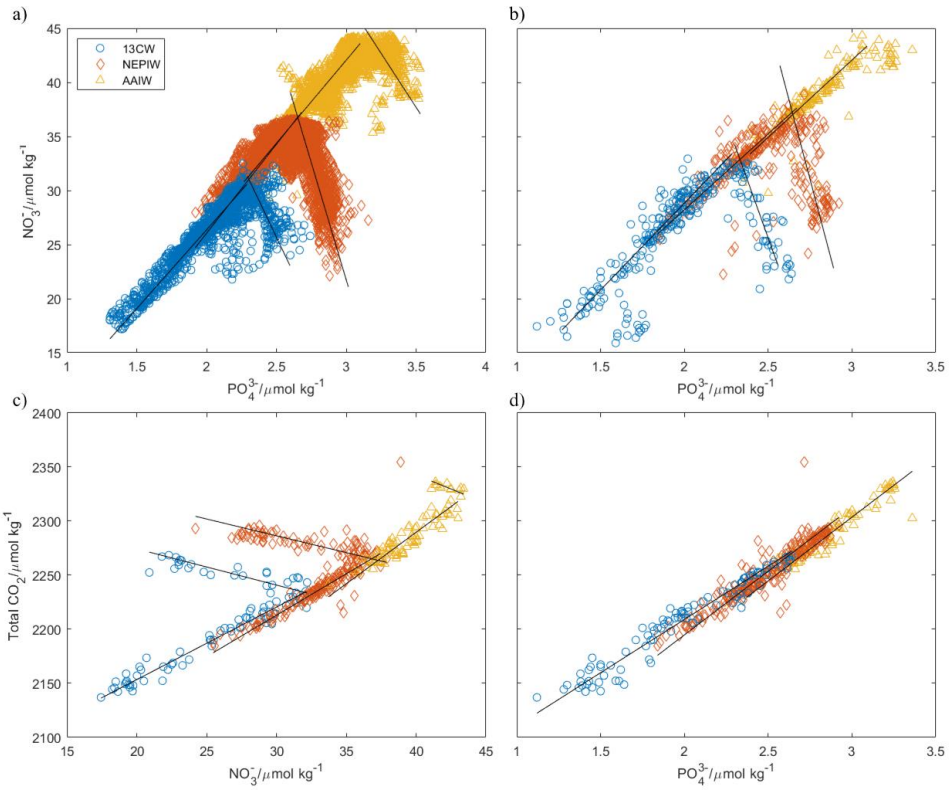

Fig. 2) Evolution of nutrients within the 13CW, NEPIW, and AAIW in the northern hemisphere using (a) NO_3^-/µmol kg^{-1} vs PO_4^{3-}/µmol kg^{-1} from WOA13, (b) NO_3^-/µmol kg^{-1} vs PO_4^{3-}/µmol kg^{-1} from WOD18 for comparison with WOA13, (c) total CO_2/µmol kg^{-1} vs NO_3^-/µmol kg^{-1} from WOD18, and (d) total CO_2/µmol kg^{-1} vs PO_4^{3-}/µmol kg^{-1} from WOD18.

Data Source	Water mass	Nutrients	Respiration	Slope
WOA13	13CW	NO_3^-:PO_4^{3-}	Anaerobic	-20±1
	NEPIW	NO_3^-:PO_4^{3-}	Anaerobic	-43±1
	AAIW	NO_3^-:PO_4^{3-}	Anaerobic	-34±3
WOD18	13CW	NO_3^-:PO_4^{3-}	Anaerobic	-43±4
	NEPIW	NO_3^-:PO_4^{3-}	Anaerobic	-59±6
	13CW	Total CO_2:NO_3^-	Anaerobic	-3±0.4
	NEPIW	Total CO_2:NO_3^-	Anaerobic	-3±0.2
	13CW	Total CO_2:PO_4^{3-}	Aerobic	99±2
	NEPIW	Total CO_2:PO_4^{3-}	Aerobic	118±3
	AAIW	Total CO_2:PO_4^{3-}	Aerobic	118±4
Froelich et al. (1979)		NO_3^-:PO_4^{3-}	Anaerobic	-94.4
		Total CO_2:NO_3^-	Anaerobic	-1.12
		Total CO_2:PO_4^{3-}	Anaerobic	106

Table 2) Ratios of nutrients depicted in Fig. 1 using linear fits and reaction stoichiometry for comparison.

The approximate phosphate concentrations where anaerobic processes begin is defined as where the nitrate:phosphate stoichiometry deviates from 16:1 in Fig. 2a. These concentrations are plotted as in Fig. 1 to visualize the approximate range where each water mass contains the signal of denitrification. Previous analysis of these water masses in Evans et al. (2020) focused on the northern part of the ETNP ODZ, where the 13CW is truly anoxic and facilitates nitrite accumulation within the slightly deeper secondary nitrite maximum, whereas the NEPIW interferes with nitrite accumulation, likely due to the fact that it is barely oxic with ~10 nM oxygen (Revsbech et al. 2009). In this northern region of the ETNP ODZ, they found that the AAIW is hypoxic. Contradictory to these results, WOA13 data reveals that denitrification has occurred in the NEPIW and even the AAIW. Since the NEPIW is introduced into the north side of the ETNP ODZ (Margolskee et al. 2019), this water mass is likely driven to anoxia as it migrates southeast through the ETNP ODZ. Nitrite data from the Costa Rica Dome (Buchwald et al. 2015; Chronopoulou et al. 2017) supports this geographical differentiation in water mass oxygen

availability, as nitrite accumulates far deeper in the south of the ETNP ODZ than the north (Evans et al. 2020). Elevated phosphate concentrations in Fig. 1c indicate that in the AAIW, this denitrification signal intensifies within the southern portion of the ETNP ODZ, where the ETNP ODZ is deeper.

We observe the largest nitrate:phosphate slope for the 13CW using the WOA13 dataset. The 13CW is the shallowest water mass and it can shoal into the photic zone, enabling microaerophilic production of oxygen (Tiano et al. 2014). Nitrite oxidation is reported to be responsible for 40%-80% of the oxygen consumption in the edge of the ETNP ODZ (Beman et al. 2021), and this fact supports the significant fraction of nitrite oxidation observed in the 13CW using the WOA13 dataset. A similar trend can be seen in the nitrate:phosphate slopes for the 13CW and NEPIW in the WOD18 data, though these values are closer to the stoichiometric estimate of -94.4. The anaerobic portion of the WOD18 data originates solely from cruises on the CLIVAR P18 line. This repeat transect occupies 110 ºW and therefore bisects through the middle of the ETNP ODZ (Fig. S1), emphasizing the processes within the oxygen deficient layer. The WOA13 gridded data encompasses the ETNP ODZ causing its boundaries to be well-represented in this dataset, leading to the higher impact of microaerobic regions on nitrite oxidation.

Future and global implications

We can estimate the percent of nitrite that is re-oxidized in the ETNP by comparing the WOD18 data against the expected -1.12 total inorganic carbon:nitrate ratio and the WOA13 data against the -94.4 nitrate:phosphate ratio. In the case of Eq. 1, which compares carbon:nitrate ratios, the difference between the observed -3 and the expected -1.12 was found, then scaled by the observed value to determine the precent difference. This comparison is more accurate than the nitrate:phosphate comparison because the carbon:nitrate ratio is less sensitive to artificial adjustment by other metabolisms. Unfortunately, the carbon data in this region is limited, so we compared nitrate:phosphate as well. These comparisons reveal that within the core of the ETNP ODZ, as sampled by the WOD18 data, 66±12% of the nitrite produced is re-oxidized. This estimate is similar to a previous study that found 50% nitrite re-oxidation (Buchwald et al. 2015) as well as another study that found nitrite oxidation rates exceeded nitrate reduction rates (Babbin et al. 2020). Extending this data to the entire ETNP, presented with WOA13 data in Table 2, reveals that the 13CW contains 79±7% nitrite oxidation, which is noticeably higher than previous estimates.

Interestingly, the nitrate:phosphate slopes of the 13CW and NEPIW differ significantly in the WOD18 dataset, whereas their carbon:nitrate slopes are statistically equivalent. The differences in the carbon:phosphate slopes cause the nitrate:phosphate slopes to differ from the carbon:nitrate slopes for this dataset. Nevertheless, nitrite oxidation is likely highest in the 13CW in the WOA13 because previous studies have also noted that the upper oxycline contains higher measured nitrite oxidation rates than the oxygen deficient layer (Peng et al. 2015), and the WOA13 dataset contains the entire upper oxycline in the ETNP ODZ.

Data source	Water mass	Nitrite oxidized (%)
WOD18	13CW	66±12
	NEPIW	64±8
WOA13	13CW	79±7
	NEPIW	54±2
	AAIW	64±9

Table 3) Percent of nitrite re-oxidized based on slopes fit in Table 2.

These significant proportions of nitrite re-oxidation indicate that steady-state nitrate and phosphate concentrations cannot indicate the rate or extent of nitrate reduction without a 54%-79% correction, depending on location within the ETNP. Inverse modeling of ODZs requires nitrite oxidation closely paired with nitrate reduction to maintain realistic concentration and isotope distributions (Martin et al. 2019) or artificially lower remineralization rates to prevent nitrate depletion (Su et al. 2015). Models that simulate fixed nitrogen loss using N* without including prolific and depth-dependent nitrite re-oxidation (Deutsch et al. 2001; Codispoti et al. 2001; DeVries et al. 2013) likely overestimate the fixed nitrogen loss within marine ODZs. Fu et al. (2018) predicts that ODZs will expand until approximately 2100 then contract, but these calculations rely on a fixed stoichiometry and increasing the oxycline area of the 13CW may alter the amount of nitrite denitrified versus recycled.

This study is the first effort to use basin-wide data to determine the partitioning of nitrite between reduction and oxidation rather than extrapolating from a subset of points or matching data with models. This approach suffers from significant scatter in water mass data, causing large uncertainties, though these uncertainties may be derived from the fact that the nitrite re-oxidation

varies widely across the ETNP. Ultimately, sparse measurements of both inorganic nitrogen and carbon parameters within Pacific ODZs limit the ability to derive robust conclusions. This large scale data manipulation also cannot determine the reducing agent for nitrite oxidation, though oxygen, iodate, and even nitrite dismutation have been proposed (Babbin et al. 2020; Sun et al. 2021). We calculate that between 54%-79% of nitrite produced in the ETNP is re-oxidized, with 64±8% in the core of the ETNP ODZ. We find the highest nitrite oxidation in the shallow 13CW because this water mass contains microaerobic pockets due to the secondary chlorophyll maximum as well as high respiration rates. This analysis demonstrates the significance of nitrite recycling, which exceeds nitrite loss across the ETNP ODZ, and the impact of this recycling on elevating phosphate comparisons. Most importantly, the disconnect between nitrate reduction rates from concentrations of nitrate and phosphate influences how oceanographers and ocean modelers represent fixed nitrogen loss in the ocean.

Acknowledgements

N.E. and J.W.M. were supported by NSF OCE 2023708 and J.T. was supported by the University of Southern California Wrigley REU program. We would like to acknowledge the extensive programs that went into compiling the World Ocean Atlas and World Ocean Database such that these resources could be publicly available. Subsets of these datasets used for this analysis, as well as the code for processing them, is available at https://github.com/NatalyaEvans/ETNP_stoich. Amanda Taing provided copy edits for this manuscript.

Author contributions

N.E. designed this study, acquired the data, trained J.T., and wrote this manuscript. J.T. did the primary analysis of these data sets. J.W.M. advised throughout and A.D. framed this research within the current state of the field.

Competing interests

The authors declare no competing interests.

References

Anderson, J. J., A. Okubo, A. S. Robbins, and F. A. Richards. 1982. A model for nitrate distributions in oceanic oxygen minimum zones. Deep Sea Research Part A. Oceanographic Research Papers **29**: 1113–1140. doi:10.1016/0198-0149(82)90031-0

Babbin, A. R., C. Buchwald, F. M. M. Morel, S. D. Wankel, and B. B. Ward. 2020. Nitrite oxidation exceeds reduction and fixed nitrogen loss in anoxic Pacific waters. Marine Chemistry **224**: 103814. doi:10.1016/j.marchem.2020.103814

Babbin, A. R., B. D. Peters, C. W. Mordy, B. Widner, K. L. Casciotti, and B. B. Ward. 2017. Multiple metabolisms constrain the anaerobic nitrite budget in the Eastern Tropical South Pacific: Nitrogen Dynamics in the Eastern Tropical South Pacific. Global Biogeochemical Cycles. doi:10.1002/2016GB005407

Beman, J. M., S. M. Vargas, J. M. Wilson, and others. 2021. Substantial oxygen consumption by aerobic nitrite oxidation in oceanic oxygen minimum zones. Nat Commun **12**: 7043. doi:10.1038/s41467-021-27381-7

Bostock, H. C., B. N. Opdyke, and M. J. M. Williams. 2010. Characterising the intermediate depth waters of the Pacific Ocean using δ13C and other geochemical tracers. Deep Sea Research Part I: Oceanographic Research Papers **57**: 847–859. doi:10.1016/j.dsr.2010.04.005

Bostock, H. C., P. J. Sutton, M. J. M. Williams, and B. N. Opdyke. 2013. Reviewing the circulation and mixing of Antarctic Intermediate Water in the South Pacific using evidence from geochemical tracers and Argo float trajectories. Deep Sea Research Part I: Oceanographic Research Papers **73**: 84–98. doi:10.1016/j.dsr.2012.11.007

Brandes, J. A., and A. H. Devol. 2002. A global marine-fixed nitrogen isotopic budget: Implications for Holocene nitrogen cycling. Global Biogeochemical Cycles **16**: 67-1-67–14. doi:10.1029/2001GB001856

Buchwald, C., A. E. Santoro, R. H. R. Stanley, and K. L. Casciotti. 2015. Nitrogen cycling in the secondary nitrite maximum of the eastern tropical North Pacific off Costa Rica: NITROGEN CYCLING IN THE SNM. Global Biogeochemical Cycles **29**: 2061–2081. doi:10.1002/2015GB005187

Casciotti, K. L., C. Buchwald, and M. McIlvin. 2013. Implications of nitrate and nitrite isotopic measurements for the mechanisms of nitrogen cycling in the Peru oxygen deficient zone. Deep Sea Research Part I: Oceanographic Research Papers **80**: 78–93. doi:10.1016/j.dsr.2013.05.017

Chang, B. X., J. R. Rich, A. Jayakumar, H. Naik, A. K. Pratihary, R. G. Keil, B. B. Ward, and A. H. Devol. 2014. The effect of organic carbon on fixed nitrogen loss in the eastern tropical South Pacific and Arabian Sea oxygen deficient zones. Limnology and Oceanography **59**: 1267–1274. doi:10.4319/lo.2014.59.4.1267

Chronopoulou, P.-M., F. Shelley, W. J. Pritchard, S. T. Maanoja, and M. Trimmer. 2017. Origin and fate of methane in the Eastern Tropical North Pacific oxygen minimum zone. The ISME Journal **11**: 1386–1399. doi:10.1038/ismej.2017.6

Codispoti, L. A., J. A. Brandes, J. P. Christensen, A. H. Devol, S. W. A. Naqvi, H. W. Paerl, and T. Yoshinari. 2001. The oceanic fixed nitrogen and nitrous oxide budgets: Moving targets as we enter the anthropocene? Scientia Marina **65**: 85–105. doi:10.3989/scimar.2001.65s285

Crameri, F., G. E. Shephard, and P. J. Heron. 2020. The misuse of colour in science communication. Nature Communications **11**: 5444. doi:10.1038/s41467-020-19160-7

Deutsch, C., N. Gruber, R. M. Key, J. L. Sarmiento, and A. Ganachaud. 2001. Denitrification and N2 fixation in the Pacific Ocean. Global Biogeochemical Cycles **15**: 483–506. doi:10.1029/2000GB001291

DeVries, T., C. Deutsch, P. A. Rafter, and F. Primeau. 2013. Marine denitrification rates determined from a global 3-D inverse model. Biogeosciences **10**: 2481–2496. doi:10.5194/bg-10-2481-2013

DiSpirito, A. A., and A. B. Hooper. 1986. Oxygen exchange between nitrate molecules during nitrite oxidation by Nitrobacter. Journal of Biological Chemistry **261**: 10534–10537. doi:10.1016/S0021-9258(18)67417-4

Evans, N., E. Boles, J. V. Kwiecinski, and others. 2020. The role of water masses in shaping the distribution of redox active compounds in the Eastern Tropical North Pacific oxygen deficient zone and influencing low oxygen concentrations in the eastern Pacific Ocean. Limnology and Oceanography **65**: 1688–1705. doi:10.1002/lno.11412

Fiedler, P. C., and L. D. Talley. 2006. Hydrography of the eastern tropical Pacific: A review. Progress in Oceanography **69**: 143–180. doi:10.1016/j.pocean.2006.03.008

Froelich, P. N., G. P. Klinkhammer, M. L. Bender, and others. 1979. Early oxidation of organic matter in pelagic sediments of the eastern equatorial Atlantic: suboxic diagenesis. Geochimica et Cosmochimica Acta **43**: 1075–1090. doi:10.1016/0016-7037(79)90095-4

Fu, W., F. Primeau, J. Keith Moore, K. Lindsay, and J. T. Randerson. 2018. Reversal of Increasing Tropical Ocean Hypoxia Trends With Sustained Climate Warming. Global Biogeochemical Cycles **32**: 551–564. doi:10.1002/2017GB005788

Garcia, H. E., T. P. Boyer, R. A. Locarnini, and others. 2013. World ocean atlas 2013. Volume 3, Dissolved oxygen, apparent oxygen utilization, and oxygen saturation.doi:10.7289/V5XG9P2W

Garcia-Robledo, E., A. Paulmier, S. M. Borisov, and N. P. Revsbech. Sampling in low oxygen aquatic environments: The deviation from anoxic conditions. Limnology and Oceanography: Methods **n/a**. doi:10.1002/lom3.10457

Glover, D. M., W. J. Jenkins, and S. C. Doney. 2011. Modeling Methods for Marine Science, Cambridge University Press.

Gruber, N., and J. L. Sarmiento. 1997. Global patterns of marine nitrogen fixation and denitrification. Global Biogeochemical Cycles **11**: 235–266. doi:10.1029/97GB00077

Hernandez-Ayon, J. M., A. Paulmier, V. Garcon, and others. 2019. Dynamics of the Carbonate System Across the Peruvian Oxygen Minimum Zone. Frontiers in Marine Science **6**.

Kraft, B., N. Jehmlich, M. Larsen, L. A. Bristow, M. Könneke, B. Thamdrup, and D. E. Canfield. 2022. Oxygen and nitrogen production by an ammonia-oxidizing archaeon. Science. doi:10.1126/science.abe6733

Kwiecinski, J. V., and A. R. Babbin. 2021. A High-Resolution Atlas of the Eastern Tropical Pacific Oxygen Deficient Zones. Global Biogeochemical Cycles **35**: e2021GB007001. doi:10.1029/2021GB007001

Lipschultz, F., S. C. Wofsy, B. B. Ward, L. A. Codispoti, G. Friedrich, and J. W. Elkins. 1990. Bacterial transformations of inorganic nitrogen in the oxygen-deficient waters of the Eastern Tropical South Pacific Ocean. Deep Sea Research Part A. Oceanographic Research Papers **37**: 1513–1541. doi:10.1016/0198-0149(90)90060-9

Margolskee, A., H. Frenzel, S. Emerson, and C. Deutsch. 2019. Ventilation Pathways for the North Pacific Oxygen Deficient Zone. Global Biogeochemical Cycles **33**: 875–890. doi:10.1029/2018GB006149

Martin, T. S., F. Primeau, and K. L. Casciotti. 2019. Assessing Marine Nitrogen Cycle Rates and Process Sensitivities With a Global 3-D Inverse Model. Global Biogeochemical Cycles **33**: 1026–1047. doi:10.1029/2018GB006088

Peng, X., C. A. Fuchsman, A. Jayakumar, S. Oleynik, W. Martens-Habbena, A. H. Devol, and B. B. Ward. 2015. Ammonia and nitrite oxidation in the Eastern Tropical North Pacific. Global Biogeochemical Cycles **29**: 2034–2049. doi:10.1002/2015GB005278

Qiu, B., D. L. Rudnick, S. Chen, and Y. Kashino. 2013. Quasi-stationary North Equatorial Undercurrent jets across the tropical North Pacific Ocean. Geophysical Research Letters **40**: 2183–2187. doi:10.1002/grl.50394

Qu, T., and E. J. Lindstrom. 2004. Northward Intrusion of Antarctic Intermediate Water in the Western Pacific. Journal of Physical Oceanography **34**: 2104–2118. doi:10.1175/1520-0485(2004)034<2104:NIOAIW>2.0.CO;2

Revsbech, N. P., L. H. Larsen, J. Gundersen, T. Dalsgaard, O. Ulloa, and B. Thamdrup. 2009. Determination of ultra-low oxygen concentrations in oxygen minimum zones by the STOX sensor. Limnology and Oceanography: Methods **7**: 371–381. doi:10.4319/lom.2009.7.371

Schlitzer, R. 2020. Ocean Data View.doi:odv.awi.de, 2020

Su, B., M. Pahlow, H. Wagner, and A. Oschlies. 2015. What prevents nitrogen depletion in the oxygen minimum zone of the eastern tropical South Pacific? Biogeosciences **12**: 1113–1130. doi:10.5194/bg-12-1113-2015

Sun, X., C. Frey, E. Garcia-Robledo, A. Jayakumar, and B. B. Ward. 2021. Microbial niche differentiation explains nitrite oxidation in marine oxygen minimum zones. The ISME Journal 1–13. doi:10.1038/s41396-020-00852-3

T. J. McDougall, and P. M. Barker. 2011. Getting started with TEOS-10 and the Gibbs Seawater (GSW) Oceanographic Toolbox, SCOR/IAPSO WG127.

The MathWorks, Inc. 2018. MATLAB Release 2018b,.

Tiano, L., E. Garcia-Robledo, T. Dalsgaard, A. H. Devol, B. B. Ward, O. Ulloa, D. E. Canfield, and N. Peter Revsbech. 2014. Oxygen distribution and aerobic respiration in the north and south eastern tropical Pacific oxygen minimum zones. Deep-Sea Research Part I: Oceanographic Research Papers **94**: 173–183. doi:10.1016/j.dsr.2014.10.001

Van Mooy, B. A. S., R. G. Keil, and A. H. Devol. 2002. Impact of suboxia on sinking particulate organic carbon: Enhanced carbon flux and preferential degradation of amino acids via denitrification. Geochimica et Cosmochimica Acta **66**: 457–465. doi:10.1016/S0016-7037(01)00787-6

Supplemental information

WOA13 and WOD18 data needed to be subset into the water masses supplying the ODZ to analyze these nutrient relationships. Table 1 depicts the ranges used to subset these data. Table S1 depicts all the linear fits from this data with additional significant figures. Water masses were subset using the ranges presented in Table 1. All code and data for this project can be found at https://github.com/NatalyaEvans/ETNP_stoich.

Data Source	Nutrients	Water mass	Respiration	Slope	Error	Intercept	Error
WOA13	NO3-PO4	13CW	Aerobic	15.38	0.13	-4.07	0.23
WOA13	NO3-PO4	13CW	Anaerobic	-19.93	1.41	107.43	2.53
WOA13	NO3-PO4	NEPIW	Aerobic	16.44	0.28	-6.83	0.44
WOA13	NO3-PO4	NEPIW	Anaerobic	-43.33	1.06	151.71	1.76
WOA13	NO3-PO4	AAIW	Aerobic	14.44	0.12	-2.34	0.17
WOA13	NO3-PO4	AAIW	Anaerobic	-34.23	3.11	110.80	4.84
WOA13	SiO4-PO4	13CW	Aerobic	11.92	0.33	-1.09	0.47
WOA13	SiO4-PO4	NEPIW	Aerobic	18.77	0.28	-9.71	0.44
WOA13	SiO4-PO4	AAIW	Aerobic	48.13	0.73	-64.02	1.25
WOD18	NO3-PO4	13CW	Aerobic	16.06	0.36	-3.29	0.50
WOD18	NO3-PO4	13CW	Anaerobic	-43.18	4.03	133.55	6.31
WOD18	NO3-PO4	NEPIW	Aerobic	14.05	0.41	0.12	0.63
WOD18	NO3-PO4	NEPIW	Anaerobic	-58.54	6.10	191.99	10.08
WOD18	NO3-PO4	AAIW	Aerobic	14.29	0.50	-0.80	0.83
WOD18	C-PO4	13CW	Aerobic	98.53	2.43	2012.04	3.55
WOD18	C-PO4	NEPIW	Aerobic	117.89	2.96	1959.06	4.71
WOD18	C-PO4	AAIW	Aerobic	117.92	3.94	1949.92	6.72
WOD18	C-NO3	13CW	Aerobic	6.70	0.18	2019.44	1.20
WOD18	C-NO3	13CW	Anaerobic	-3.35	0.41	2341.27	2.49
WOD18	C-NO3	NEPIW	Aerobic	7.66	0.23	1983.19	1.39
WOD18	C-NO3	NEPIW	Anaerobic	-3.11	0.25	2379.70	1.57
WOD18	C-NO3	AAIW	Aerobic	9.51	0.44	1909.30	2.88
ESM4	NO3-PO4	13CW	Aerobic	14.58	0.01	1.08	0.02
ESM4	NO3-PO4	13CW	Anaerobic	-51	1.0	142.7	1.5
ESM4	NO3-PO4	NEPIW	Aerobic	13.717	0.006	2.160	0.008
ESM4	NO3-PO4	NEPIW	Anaerobic	-70.90	0.53	224.44	0.88
ESM4	NO3-PO4	AAIW	Aerobic	11.502	0.016	6.567	0.027
ESM4	NO3-PO4	AAIW	Anaerobic	-89.82	0.29	332.35	0.53

Table S1) Ratios of nutrients depicted in Fig. 1 using linear fits and reaction stoichiometry for comparison.

Carbon data in the Pacific ODZs, is quite limited, unlike WOA13. The map in Fig. S1 depicts where WOD18 data extracted with the WOD18select tool was sampled, and the data in Fig. 2 originates from overlap in the geographical extent of each water mass (Fig. 1) and the WOD18 carbon sampling (Fig. S1).

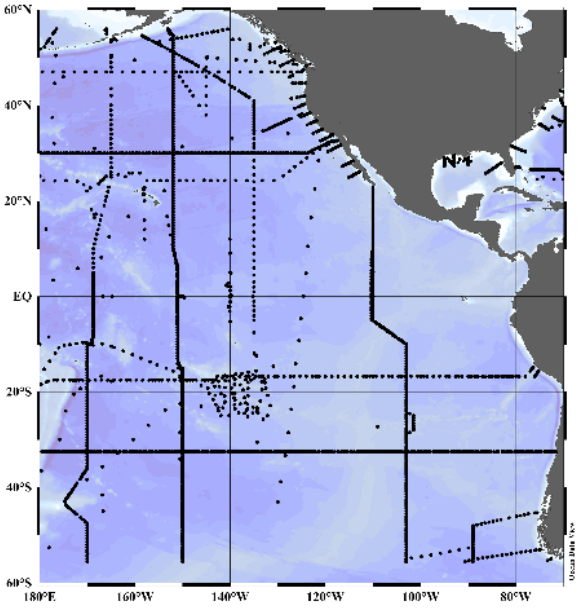

Fig. S1) Map of all WOD18 data extracted with the WOD18select tool.